THE NAMURU RECEIVER AS DEVELOPMENT PLATFORM FOR SPACEBORNE GNSS APPLICATIONS

Andreas Grillenberger[1], **Rodrigo Rivas**[1], **Markus Markgraf**[1],
Peter Mumford[2], **Kevin Parkinson**[2], **Chris Rizos**[2]

[1]*Deutsches Zentrum für Luft- und Raumfahrt (DLR)*
German Space Operations Center (GSOC)
82234 Wessling, Germany
Email: andreas.grillenberger@dlr.de

[2] *University of New South Wales*
Surveying and Spatial Information Systems
Sydney NSW 2052, Australia
Email: p.mumford@unsw.edu.au

Abstract

GPS is a well established navigation system in current spaceflight missions. Affordable GPS receivers for small satellite and sounding rocket missions are usually based on Commercial Off The Shelf (COTS) products. Many of these receivers are limited to single frequency tracking and utilise custom ASICs for the signal processing. The Phoenix receiver is an example of a commercially available receiver with custom software modifications by DLR. This receiver is based on the GP2021 baseband processor and is therefore not flexible enough to implement anything else besides GPS L1 tracking. To overcome this limitation it has been decided to migrate to the Namuru GNSS receiver platform for the development of new GNSS applications. The Namuru system is based on a reconfigurable FPGA and has been developed by the University of New South Wales (UNSW). This platform allows the baseband processing hardware to be completely customised and allows the implementation of software for different areas of research. The DLR's research projects aim at multiple frontend systems, new signals and spaceborne GNSS reflectometry. As a first step we have ported the flight proven Phoenix software to the Namuru receiver. The accuracy of the navigation solution has been validated in both low earth orbit and ballistic rocket simulations and a comparison with the Phoenix receiver is shown. In the second step, an antenna array system for spaceborne GNSS reflectometry is being implemented. Narrowband Beamforming is performed after carrier demodulation or PRN correlation, significantly lowering the requirements for the analogue front-end and at the same time allowing the use of already space proven hardware and software GPS architecture available at our department. The paper provides a description of the Namuru development board and preliminary results obtained in a signal simulation test bed. In addition, ongoing developments for special applications such as GNSS reflectometry are addressed.

1 Introduction

Global Positioning System (GPS) receivers have been used extensively in the past years for precise position and time information on spacecraft and rockets. The Space Flight Technology department of the German Aerospace Center (DLR) has developed the Phoenix GPS receiver, a custom version of the Commercial Off The Shelf (COTS) Signav MG5001 receiver. The software of this receiver has been modified to accommodate the high speed and dynamics on satellite and sounding rocket platforms, while the hardware has undergone intensive validation in thermal vacuum [1] and radiation tests [2]. In recent years the applications of GPS have been extended to reflectometry and occultation measurements, and the near future will bring new Global Navigation Satellite Systems (GNSS) and navigation signals. This includes the modernised GPS signals, the European Galileo, the Russian Glonass and the Chinese Compass systems. All these signals require new hardware and software implementations. The current mass-market receivers are therefore not capable of tracking any of the new signals. In order to be flexible enough in this changing environment, DLR has chosen the

reconfigurable Namuru GNSS Development Receiver for research and development of spaceborne and sounding rocket GNSS applications.

2 The Namuru Development Receiver

The Namuru V2 Receiver has been developed at the University of New South Wales (UNSW) in Sydney, Australia [3]. The receiver uses an Altera CycloneII Field Programmable Array (FPGA) chip for the integration of the baseband processing module and the microprocessor. Both frontends use the Zarlink GP2015 RF chip for GPS L1 at 1575.42MHz, one frontend can be configured to GPS L2 by using an onboard upconverter circuit. The board offers one USB 2.0 and two RS232 interfaces, 64MB SDRAM and 8MB flash memory. See Fig. 1 for details on the receiver. The baseband processor and the NiosII soft-core CPU are implemented in the FPGA. This allows to change the baseband processor and the CPU and adapt it to specific needs. The baseband processor has been designed by UNSW and is public domain. It is

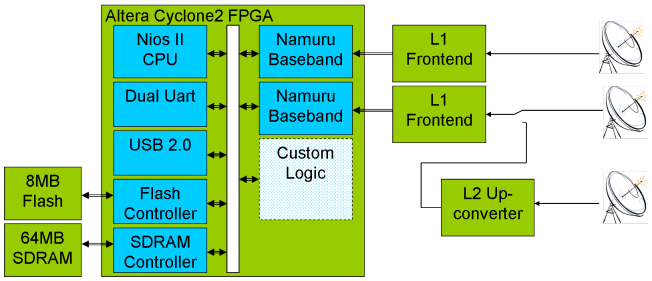

Fig. 1: Block diagram of the Namuru V2 receiver

a simplistic serial search L1 C/A code correlator module which is similar to the Zarlink GP4020 design.
A customised version of the Mitel GPS Architect software is used for the receiver, which has been ported by UNSW to run on the NiosII CPU and the Namuru baseband processor. We have further adapted the software and included the modifications that were developed for the Phoenix receiver. This allows to use the Namuru as testbed for spaceborne and sounding rocket GNSS research and development. The hardware is neither space qualified nor tested in terms of thermal vacuum and radiation tolerance, current testing is limited to a lab environment using signal simulators.

3 Performance Evaluation

The tests were performed using a Spirent STR4500 GPS signal simulator which provides L1 signals of up to 12 satellites. A Namuru and a Phoenix receiver are connected via a power divider and a low noise amplifier to the simulator. As the receiver hardware is similar to the Sigtec MG5001 used for the Phoenix receiver, the results are expected to be comparable. The simulation is based on the same scenario as used for previous Phoenix tests. The scenario simulates a sun-synchronous dusk-dawn orbit with 18h local time at the ascending node and 390km altitude. The epoch is 1 October 2008, 0:00 GPS Time and coincides with the descending node crossing. The GPS constellation is based on the GPS almanac for Week 1333. The antenna pattern is based on measurements of the Seavey SPA-16C/S antenna. The ionosphere model and broadcast ephemeris errors are disabled in the test runs.
Peak C/N_0 values of up to 46dBHz are observed in the simulations. The observed values in Fig. 2 closely match that of the reference receiver. Open air tests show a 3dB higher value, however the default power of the signal simulator [4] is about 3dB lower than the average GPS signal power. The simulation is using a discretised antenna diagram with a discretisation interval of 5° elevation. This means that the signal power at the receiver will exhibit a discrete behaviour as the boresight angle of the antenna with respect to the GPS satellite changes. The simulated antenna is zenith-pointing at all times, so the discretisation steps are observed at regular 5° intervals. The tracking is limited by the preconfigured 5° elevation mask at about 34dBHz.
The Namuru receiver tracks an average of 10 GPS satellites in the test scenario and shows a highly symmetric distribution of tracked satellites in the plane of sky. Tracking of satellites is properly stopped below the 5° elevation threshold.

3.1 Raw Measurement Accuracy

To obtain meaningful figures, double differences are used to determine the accuracy of the raw measurements. In order to limit the effect of different receiver hardware, two consecutive runs with the same receiver are recorded. The notations for the pseudorange for the same PRN in run 1 and 2 are given in (1) and (2). The true range is denoted by r, the receiver and satellite clock biases by δt_{R1} and δt_S, the simulator clock error δt_{Sim1}, the ionospheric and stratospheric errors by I and T and the receiver noise by ε_1.

$$\rho_1 = r + c_0(\delta t_{R1} - \delta t_S - \delta t_{Sim1}) + I + T + \varepsilon_1 \tag{1}$$

$$\rho_2 = r + c_0(\delta t_{R2} - \delta t_S - \delta t_{Sim2}) + I + T + \varepsilon_2 \tag{2}$$

For the virtual zero-baseline test with two consecutive runs, the satellite clock biases are identical and therefore are dropped in the formation of the single differences. By subtracting (1) from (2), the single differences are formed. Equation (3) shows the resulting single difference, note that the simulator clock error is not dropped here as it should have been using a single run with two receivers.

$$\Delta\rho_{12} = c_0(\delta t_{R1} - \delta t_{R2} + \delta t_{Sim2} - \delta t_{Sim1}) + \varepsilon_1 - \varepsilon_2 \tag{3}$$

The simulator clock error originates in an error of its frequency reference. There is only one reference in the simulator, which makes the error the same on all channels. Therefore it is removed by forming the double differences between PRN *a* and PRN *b* in (4), leaving just the receiver noise errors.

$$\nabla\Delta\rho_{12} = \varepsilon_{1a} - \varepsilon_{1b} + \varepsilon_{2a} - \varepsilon_{2b} \tag{4}$$

The virtual zero-baseline test [5] uses data collected in two consecutive 12h runs of the signal simulator. The data is used to calculate the raw measurement noise of the receiver. Fig. 3 shows the noise averaged into 0.5dBHz bins. The results are consistent with a Delay Locked Loop (DLL) and Phase Locked Loop (PLL) bandwidth of 0.065Hz and 7.5Hz respectively. The Phoenix receiver exhibits a slightly different behaviour with 0.09Hz and 8.0Hz for the DLL and PLL

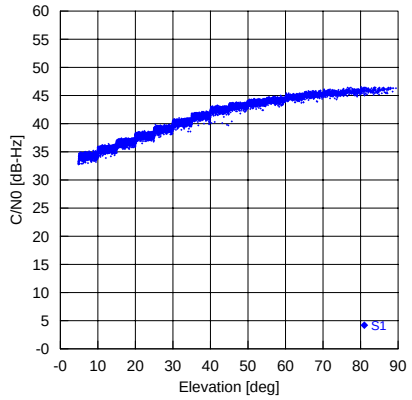

Fig. 2: Relation between carrier-to-noise-density ratio and elevation of the GPS satellites for Namuru receiver

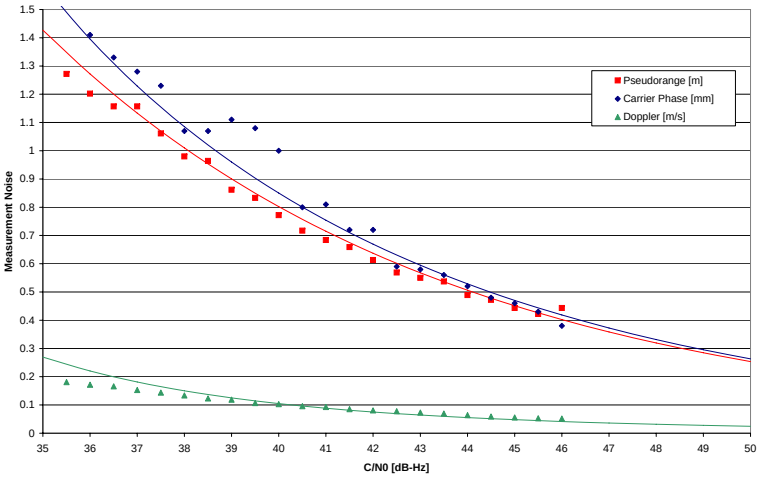

Fig. 3: Namuru receiver noise against carrier to noise density ratio

bandwidth respectively.

For a second evaluation double differences are formed against the true simulator values [6]. In this test the noise of the measurements is calculated. At a lower elevation of the two involved PRNs, a higher noise is expected due to lower C/N_0 ratios. The satellites are selected to show a representative behaviour for a low Earth orbit scenario. Fig. 4 shows an example with two satellites having similar elevations. Table 1 summarises the measurements of six selected satellite pairs with different relative velocities and elevations. The empirically determined loop bandwidths match the noise values via the relation shown in (5) [7].

$$N_0 \propto \sqrt{B} \tag{5}$$

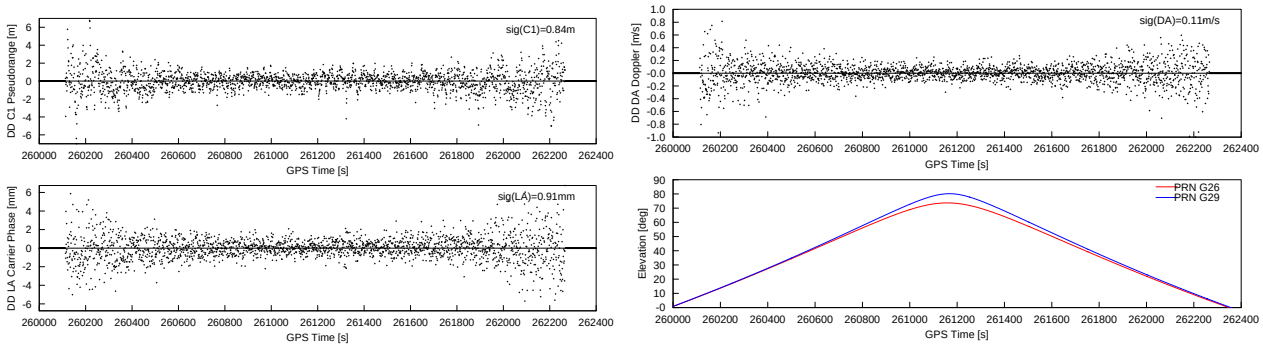

Fig. 4: Sample of double differences (PRN $26-29$, $observed-modelled$) for simultaneous visibility (C1: L1 pseudorange, LA: carrier phase, DA: Doppler).

Table 1: Standard deviation of Namuru raw data (C1: L1 pseudorange, LA: carrier phase, DA: doppler).

			Namuru			Phoenix		
Set	PRN	Tracked	C1 [m]	LA [mm]	DA [m/s]	C1 [m]	LA [mm]	DA [m/s]
1	26-29	[260113s to 260266s]	0.84	0.91	0.11	0.68	0.96	0.13
2	27-28	[260029s to 261783s]	0.85	0.97	0.12	0.68	0.98	0.13
3	2- 4	[262117s to 264157s]	1.11	1.52	0.16	0.83	1.31	0.17
4	8-10	[260569s to 261921s]	0.81	0.98	0.11	0.61	1.02	0.12
5	16-25	[264114s to 264959s]	0.89	1.05	0.12	0.65	1.14	0.14
6	19-20	[264517s to 265538s]	0.85	1.04	0.13	0.63	1.12	0.13

The table indicates that the Namuru receiver shows generally a slightly lower carrier noise than the Phoenix reference. As the doppler values are derived from the same measurements, the same behaviour can be observed. The code measurements however show a slightly increased noise.
Due to the changed correlator hardware, some changes in the receiver noise have been expected. Possible causes for the observed differences are the changed RF design and the changed Numerically Controlled Oscillators (NCO) for the code and carrier demodulation. The RF changes are expected to result in a lower noise because considerably more care has been taken in the design of the RF circuit, the NCO changes to result in a higher noise because of a decreased sensitivity of the loops. However these considerations are not consistent with the observed measurements. The different tracking loops used for the code and carrier tracking may be affected differently by the changes. The cause of the discrepancies has still to be investigated.
The observed accuracy is very close to the values observed for the reference receiver. The Namuru receiver is therefore very well suited to be used as a development platform for extending the Phoenix receivers capabilities for new applications.

3.2 Sounding Rockets

A second field of application are sounding rocket missions. The difficulties for continuous tracking is high jerk during the boost and reentry phases of the mission. A preliminary evaluation has been performed on a Maxus rocket scenario. The scenario simulates the pre-launch, boost and free-flight phases of the mission. The simulation includes ionospheric and tropospheric errors, so the absolute position accuracy is dominated by these delays. However the simulation gives a realistic figure on the real-life performance of the receiver.
A static phase on the launch pad of 180s allows the receiver to acquire satellites before launch. Lift-off is at $t = 0$s, the duration of the boost phase is 63s. The maximum acceleration of 13g is reached near the end of the boost phase. Apogee is at $t = 457$s in 713340m above ground level. Fig. 5 shows the rms errors of position and velocity between $-100\text{s} \leq t \leq 869\text{s}$ with respect to the true simulator position. During the boost phase, the velocity error shows a significant spike. This behaviour is expected due to the jerk-sensitivity of the third-order tracking loops [8]. The receiver is tracking a total of 11 satellites during the static, boost and parts of the free-flight phase without any signal drops. PRN 31 is lost near the tracking threshold at $t = 408$s and is deselected as it sets below the 5° elevation mask at $t = 650$s. A

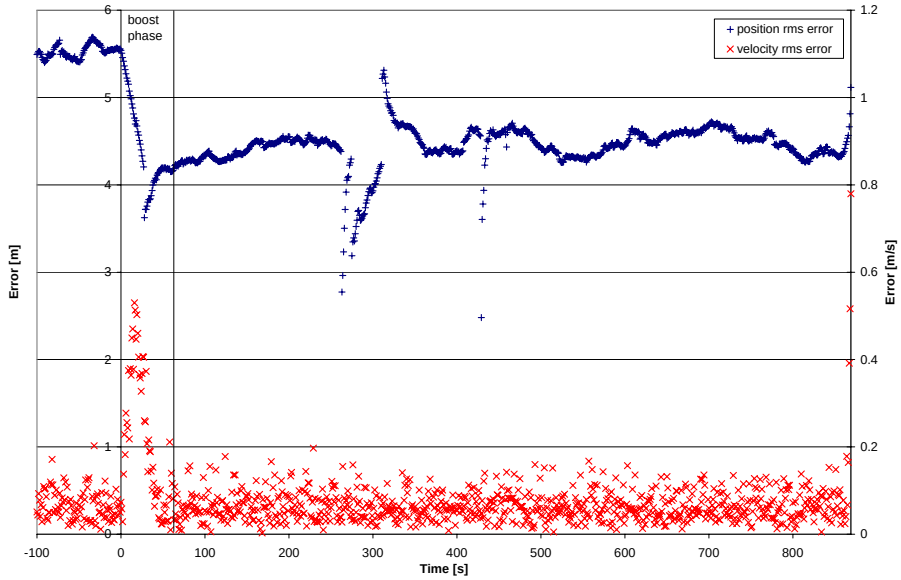

Fig. 5: 3D rms position and velocity error for the Maxus ballistic rocket scenario

jump in the position error can be observed at the point where the satellite is dropped. The outliers around $t = 580$s are probably due to a reset of the carrier phase smoothing algorithm.
The position error is below 10m and the velocity error below 1m/s during the complete simulation. This is within mission requirements of the DLR-operated sounding rockets.

4 Reflectometry/Scatterometry Receiver

The use of reflected GPS signals bounced off Earth's surface has been suggested as a new source for remote sensing technique [9] especially in the field of ocean altimetry and sea roughness surface state [10]. Its main advantages are the abundant availability of GPS signals which allows the sensing of a wider area compared with traditional active monostatic radars and the use of signals by the GPS system in the L band which is robust to weather conditions [8]. The reflectometry/scatterometry GNSS receiver is a passive instrument that has reduced size and cost, making it suitable to be deployed in several satellites as payload forming an efficient constellation for Earth remote sensing. Its main disadvantage is that the GPS signals weren't designed for this kind of applications which requires a higher bandwidth to be able to resolve with higher precision the parameters of the ocean surface.

In this frame the department of Space Flight Technology at the DLR's German Space Operations Center (GSOC) is currently developing a new Reflectometry/Scatterometry receiver. This new GNSS-R instrument is being designed to be used in several conditions ranging from terrestrial applications to spaceborne GNSS Reflectometry/Scatterometry experiments. It computes a Delay-Doppler map (through time multiplexing the Doppler space) on one reflection event at a time using a 3x3 fully digitally steerable antenna array. The specular reflection points (SRP) are dynamically computed for all available GNSS satellites based on the current host vehicle position and a suitable satellite is allocated to the Delay-Doppler processing chain based on certain configurable criteria. The available Delay-Doppler IQ output matrix could be either made available to an external user for later post-processing or it could be digitally processed in the receiver itself to extract the parameters of the signal reflection models. All this is done in real time by the receiver. A prototype version of this GNSS-R receiver is being developed as a proof of concept, using the Namuru board as development platform.

The current Namuru hardware offers a dual L1 frontend and can thus concurrently operate a zenith pointing navigation antenna as well as a left-hand circular polarized nadir pointing antenna. For beamforming, the latter string will be replaced by a 2 antenna array with associated frontends (Fig. 6). The digitized IF signal from every antenna in the antenna array is feed to the Reflectometry chains for parallel processing. To compute a Reflectometry Delay-Doppler map, the signal from the local digital carrier NCO is used to generate the Doppler space through several evenly spaced Doppler-bins. Similarly the code-delay space is generated with the digital C/A NCO operating at higher frequency than the C/A chip rate. Both, the Doppler and the code-delay space size are set dynamically by the receiver depending on the geometry of

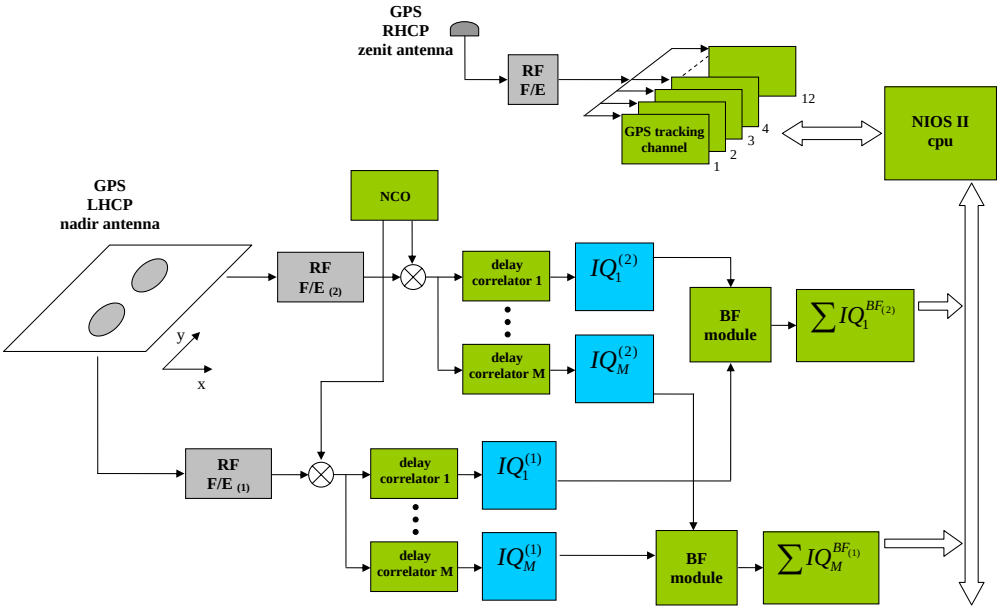

Fig. 6: Block diagram of the Namuru based Reflectometry/Scatterometry

the signal reflection and eventually on the characteristics and state of the reflecting surface. This is done so to be able to extract as much information as possible from the reflected GNSS signal. The output of every Reflectometry chain is a Delay-Doppler IQ matrix that is updated every 1ms. To synthesize the antenna array beam, digital beamforming (DBF) is preferred instead of analogue beamforming. The Phased Array Beamforming is the implemented BF algorithm and it is done at the digital-back end of the GNSS Reflectometry/Scatterometry receiver. We implement the Phased Array Beamforming after IF carrier and C/A code demodulation. This reduces significantly the technical requirements and cost of the analogue RF front-end chain and the computation bandwidth at the FPGA respectively. In this algorithm each element of the Delay-Doppler IQ matrix is rotated and multiplied by a factor before being mixed with the Delay-Doppler IQ matrix of the corresponding Reflectometry chain of every other antenna. This then produces the result of one antenna array beam steered to the desired SRP. This Delay-Doppler IQ matrix is then incoherently accumulated over a period ranging from 1ms to several seconds. This period of accumulation is also set dynamically by the receiver. The output of this accumulation process is then either made available to the input of the digital signal processing HDL modules in charge of the model parameter extraction or is downloaded to an external device for post-processing.

Even when the antenna array of this prototype using the Namuru II board comprises only two GPS LHCP antenna elements, it is enough to implement, develop and test a high number of functionalities of a fully digital steerable GNSS reflectometry/scatterometry antenna array receiver and therefore it is a suitable development platform for this application.

4.1 Code Delay Space

This subsection describes the code delay space of the GNSS-R instrument. To generate this space the traditional early-prompt-late GPS C/A correlation products has to be expanded to N correlators. Since we are working with the IQ vectors, the total number of correlators to produce N points in the code delay space is $2{\cdot}N$. The Reflectometry hardware module in the FPGA internally generates a C/A code with a chip rate set by the user. A higher C/A code chip rate is needed in order to get a better resolution of the correlation function. In order words the rate of this new C/A code chips is:

$$f_\alpha = \alpha \cdot f_{C/A} \tag{6}$$

where $f_{C/A}$ is the C/A code chip rate at 1.023MHz and α is the rate factor which is bigger than one. The GPS C/A L1 code rate in equation (6) corresponds in reality to the doppler bin being used. In the case of the prompt doppler bin (the one used to track the direct GPS signal) the value of $f_{C/A}$ will be different from the nominal 1.023MHz value since the doppler due to the relative movement between the GPS satellite and the receiver has to be taken into account.
The size of the code delay space and the rate of its C/A code chip determines the span of the code delay space in distance.

In order to have an idea of the span of the code delay space with varying rate we use the equation (7) which gives the span over the GPS L1 C/A code

$$C/A\ span = \frac{N}{\alpha} \tag{7}$$

Fig. 7 shows the code space delay correlation products of the Reflectometry hardware module for GPS signal reflection test using a GPS signal simulator, which has been setup with a constant reflection distance offset of 1000m and an attenuation of 3dB.
The first correlation peak from the left corresponds to the direct GPS L1 signal, while the second highest peak corresponds to the GPS signal reflection.
The code delay space size is $N = 81$ and the C/A code chip rate used a factor of $\alpha = 8$, meaning it is 8 times faster than the GPS L1 C/A code rate or approximately 8.184MHz.

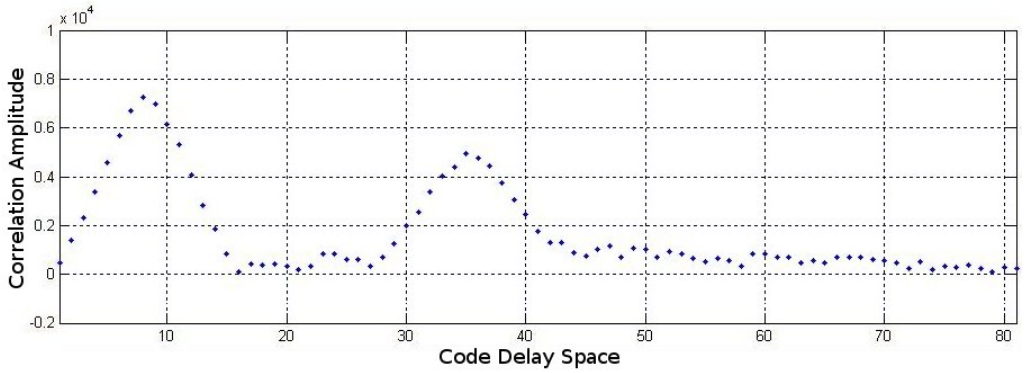

Fig. 7: Code delay space showing a GPS L1 signal reflection

The distance in the code delay space between the two maximum peaks is 27. Following equation (6) the equivalent distance in meters between two consecutive points in the code delay space is

$$d_\alpha = \frac{1}{\alpha \cdot f_{C/A}} \cdot c_0 = 36.6\text{m} \tag{8}$$

where we approximate the speed of light to the vacuum case c_0. So, the distance in meters between the two correlation peaks is approximately 989m. This result also shows that one of the main factors in the discrepancy of the measured distance of the two correlation peaks through the code delay space used in this experiment is the C/A code chip rate of the code delay space that determines the resolution of this measurement.

5 Conclusion

The Namuru Receiver has been shown to be comparable to the currently used Phoenix receiver. It is working well under the high speeds and high signal dynamics required for satellite and sounding rocket missions and therefore proved to be an excellent platform for further developments. An outline of the dedicated scatterometry and reflectometry hardware and first results have been shown.

References

[1] H. Lux, M. Markgraf, "Thermal-Vacuum Testing of the Phoenix GPS Receiver", DLR-GSOC TN 04-07, Deutsches Zentrum für Luft- und Raumfahrt, Oberpfaffenhofen, 2004

[2] M. Markgraf, O. Montenbruck, "Total Ionizing Dose Testing of the Orion and Phoenix GPS Receivers", DLR-GSOC TN 04-01, Deutsches Zentrum für Luft- und Raumfahrt, Oberpfaffenhofen, 2004

[3] P.J. Mumford, K. Parkinson, A.G. Dempster, "The Namuru Open GNSS Research Receiver", 19th Int. Tech. Meeting of the Satellite Division of the U.S. Inst. of Navigation, Fort Worth, Texas, USA, 2006

[4] ”STR4500 GPS/SBAS Simulator with SimPLEX Software User Manual“, DGP00603AAA, Issue 1.11, Jan 2005, unpublished

[5] O. Montenbruck, M. Garcia-Fernandez, J. Williams, ”Performance Comparison of Semi-Codeless GPS Receivers for LEO Satellites“, GPS Solutions 10, 249-261, 2006. DOI 10.1007/s10291-006-0025-9

[6] O. Montenbruck, G. Holt, ”Spaceborne GPS Receiver Performance Testing“, DLR-GSOC TN 02-04; Deutsches Zentrum für Luft- und Raumfahrt, Oberpfaffenhofen, 2002

[7] C.R. Cahn, D.K. Leimer, C.L. Marsh, F.J. Huntowski, G.D. Larue ”Software Implementation of a PN Spread Spectrum Receiver to Accomodate Dynamics“, IEEE Transactions on Communications, Vol. COM-25, 1977

[8] E.D. Kaplan, C.J. Hegarty ”Understanding GPS - Principles and Applications“, Artech House, 2006

[9] M. Martin-Neira ”A passive reflectometry and interferometry system (PARIS): Application to ocean altimetry“, ESA J., Vol. 17, pp. 331-355, 1993

[10] V.U. Zavorotny, A.G. Voronovich ”Scattering of GPS signals from the ocean with wind remote sensing application“, IEEE Trans. Geosci. Remote Sens., Vol. 38, no. 2, pp. 951-964, 2000